X-621-71-310
PREPRINT

MODEL FOR ROTATING AND NON-UNIFORM PLANETARY EXOSPHERES

R. E. HARTLE

AUGUST 1971

GSFC — GODDARD SPACE FLIGHT CENTER —
GREENBELT, MARYLAND

Model for Rotating and Nonuniform Planetary Exospheres

R. E. Hartle

Laboratory for Planetary Atmospheres

Goddard Space Flight Center, Greenbelt, Maryland

To appear in Physics of Fluids

GODDARD SPACE FLIGHT CENTER
Greenbelt, Maryland

ABSTRACT

The model neutral exosphere with a uniformly rotating exobase is generalized by allowing variations in exobase density and temperature which characterize the thermosphere just below the base. The corresponding velocity distribution function, satisfying the collisionless Boltzmann equation, is constructed and used to form a general expression for the velocity moments. Resulting density profiles of rotating exospheres with nonuniform densities and temperatures on the exobase are compared with corresponding nonrotating exospheres. Density enhancements due to rotation are found to be greatest above regions of exobase density or temperature minima. Equatorial density enhancements of terrestrial hydrogen, resulting from rotation, are estimated to be 15 to 17 percent at altitudes of 10 to 20 earth radii. Corresponding increases in terrestrial helium are 30 to 50 percent on the equator at altitudes of 0.7 to 1 earth radii even when there is a polar density bulge in the barosphere.

I. INTRODUCTION

The neutral planetary exosphere model of Öpik and Singer[1,2] consists of a spherical base, or exobase, of radius R, through which all particles populating the collisionless exosphere emerge with a Maxwellian velocity distribution, characterized by uniform density and temperature and no rotation (no azimuthal bulk motion). On this model, Öpik and Singer obtained an integral expression for the density profile which was subsequently confirmed by others,[3,4] through independent means, and placed in closed form. In a recent paper,[5] hereafter referred to as I, Hagenbuch and Hartle extended the model by permitting the exobase to rotate uniformly with angular velocity $\vec{\omega}$. It was found in I that important enhancements in exospheric density and escape flux on the equator (plane normal to rotation axis) can be affected by the inclusion of rotation. Burke[6] also noted increasing escape flux with rotation and discussed the possible astrophysical consequences. In addition to the rotational effects, important exospheric changes result when density and temperature variations are included on the exobase. The importance of such variations has long been recognized in the study of lateral flow in the terrestrial exosphere[7-10] (flow from regions of high to regions of low exobase densities and/or temperatures).

The purpose of this paper is to generalize the rotating exosphere model of I by allowing variations in exobase density, temperature, and bulk flow which characterize the thermosphere (barosphere) just below the exobase. We begin, in Sec. II, by constructing an explicit solution of the collisionless Boltzmann equation from which we form a general expression for the velocity moments; e.g., density, flux, temperature, etc. The moments are in quadrature form and

must be treated numerically. In section III we present density profiles for selected conditions intended to bring out the principal effects resulting from a rotating exobase with density and temperature variations. Apart from that required for rotation, we ignore exobase bulk flow as done in all models to present. However, we discuss the possible importance of such flow in the final section along with other results of the present model.

II. FORMULATION OF MODEL

The exobase surface is defined[2] by those points in the atmosphere where the lateral mean free path equals twice the density scale H; i.e., $H n \sigma = 1/2$, in terms of the density n and gas-kinetic collision cross section σ. Then, due to the assumed variations in density and temperature, the exobase is a nonspherical surface with maximum and minimum radii. However, in this treatment we assume that the exobase is a sphere of radius R lying somewhere between these extremes. We also assume that the variations in base density and temperature are weak in the sense that the resulting difference between the maximum and minimum radii is small relative to R.

We construct the velocity distribution function f in the inertial frame with a spherical coordinate system whose origin is at the center of the planet. In this case, the spatial coordinates are r, θ, and ϕ, the radial, colatitude, and azimuthal coordinates, respectively, and the corresponding Cartesian velocities are v_r, v_θ, and v_ϕ. At the exobase, $\vec{r} = \vec{R}$, the velocity distribution $f(\vec{r}, \vec{v})$ of particles emerging into the exosphere is taken to correspond to local thermodynamic equilibrium to give the boundary condition

$$f(\vec{R}, \vec{v}) = N(\theta, \phi) \left(\frac{m}{2\pi k T(\theta, \phi)} \right)^{3/2} \exp \left\{ - \frac{m[\vec{v} - \vec{U}(\theta, \phi)]^2}{2k T(\theta, \phi)} \right\} \text{ for } \vec{v} \cdot \vec{R} > 0 \quad (1)$$

in terms of the particle mass m and Boltzmann's constant k. The functional dependences of the particle density $N(\theta, \phi)$, temperature $T(\theta, \phi)$, and bulk velocity $U(\theta, \phi)$ characterizing the emergent distribution can be obtained from theoretical models or experimental data. Only simple forms for these functions are chosen in this work to illustrate the main features of this model.

The exospheric distribution function f we seek satisfies the collisionless Boltzmann equation (in inertial frame)

$$v_r \frac{\partial f}{\partial r} + \frac{v_\theta}{r} \frac{\partial f}{\partial \theta} + \frac{v_\phi}{r \sin\theta} \frac{\partial f}{\partial \phi} + \left(\frac{v_\theta^2 + v_\phi^2}{r} - \frac{dV}{dr} \right) \frac{\partial f}{\partial v_r}$$

$$+ \left(- \frac{v_r v_\theta}{r} + \cot\theta \frac{v_\phi^2}{r} \right) \frac{\partial f}{\partial v_\theta} + \left(- \frac{v_r v_\phi}{r} - \cot\theta \frac{v_\theta v_\phi}{r} \right) \frac{\partial f}{\partial v_\phi} = 0, \quad (2)$$

in which the gravitational potential

$$V = - MG/r,$$

where M is the planetary mass and G the gravitational constant. The most general solution of Eq. (2) consists of an arbitrary function of the five constants of particle motion obtained by solving the corresponding characteristic equations to give

$$E = \frac{1}{2} m \left(v_r^2 + v_\theta^2 + v_\phi^2 \right) + m V, \quad (3a)$$

$$J^2 = m^2 r^2 \left(v_\theta^2 + v_\phi^2 \right), \quad (3b)$$

$$J_z = m r \sin\theta \, v_\phi, \quad (3c)$$

$$K = \cos^{-1} \left[\frac{\cos\theta}{(1 - J_z^2/J^2)^{1/2}} \right] - \cos^{-1} \eta(r), \quad (3d)$$

$$L = \phi - \zeta(\sin^2\theta), \quad (3e)$$

where

$$\eta(x) = \frac{1 - J^2/m^2MGx}{(1 + 2EJ^2/m^3M^2G^2)^{1/2}},$$

$$\zeta(x) = \frac{1}{2}\cos^{-1}\left[\frac{(1 + J_z^2/J^2)\,x - 2J_z^2/J^2}{(1 - J_z^2/J^2)\,x}\right].$$

The first three constants are the total energy, total angular momentum squared, and the z component of the angular momentum, respectively, while the remaining two constants relate the angular coordinates of a particle trajectory.

In order to form the distribution function for the exosphere it is necessary to relate the point of observation (r, θ, ϕ) of a particle of given velocity (v_r, v_θ, v_ϕ) with the corresponding point on the exobase surface (R, Θ, Φ) where the particle emerged; i.e., the source point. Such a relationship can be represented by the expressions

$$\cos\Theta = (1 - J_z^2/J^2)\cos\left[K + \cos^{-1}\eta(R)\right], \tag{4a}$$

$$\cos\Phi = \cos\left[L + \zeta(1 - \cos^2\Theta)\right], \tag{4b}$$

in terms of the constants of motion (since Θ and Φ are functions of the constants of motion, they are constant along a particle trajectory). For a point $(\vec{v}, \vec{r})$ in phase space we note that Eqs. (4) lead to four $(E > 0)$ or eight $(E < 0)$ points (Θ, Φ). A more specific representation, required in this work, is obtained by using Eqs. (3) and (4) and following the principles of elementary orbital mechanics to give

$$\cos\Theta_{i,j} = \cos\theta\, Y_i + \epsilon_j\, P \sin\theta\, Z_i, \tag{5a}$$

$$\cos\Phi_{ijk} = \{\cos\phi\sin\theta\, Y_i - [\epsilon_j P\cos\phi\cos\theta - \epsilon_k(1-P^2)^{1/2}\sin\phi]\, Z_i\}/\sin\Theta_{ij}, \tag{5b}$$

where $\epsilon_\lambda = (-1)^{\lambda+1}$ for $\lambda = 1,2$ and the four (eight) roots $(\Theta, \Phi) \rightarrow (\Theta_{ij}, \Phi_{ijk})$ are identified by the indices (i, j, k) through $\epsilon_i = \text{sgn } v_r$, $\epsilon_j = \text{sgn } v_\theta$, and $\epsilon_k = \text{sgn } v_\phi$. The remaining functions are given by

$$P = |v_\theta| / \left(v_\theta^2 + v_\phi^2\right)^{1/2},$$

$$Y_i = \eta(R)\,\eta(r) + \epsilon_i\,\chi(R)\,\chi(r),$$

$$Z_i = \eta(r)\,\chi(R) - \epsilon_i\,\eta(R)\,\chi(r),$$

where

$$\chi(r) = [1 - \eta^2(r)]^{1/2}.$$

In addition to satisfying the boundary condition of Eq. (1), the distribution function we seek only admits particles which have emerged from the exobase and excludes those particles exceeding the escape speed with negative radial velocities (i.e., no source of particles at infinity). The distribution function we propose is

$$f = N(\Theta, \Phi) \left(\frac{m}{2\pi k\,T(\Theta, \Phi)}\right)^{3/2} \exp\left[-\frac{m\left(\vec{V} - \vec{U}(\Theta, \Phi)\right)^2}{2k\,T(\Theta, \Phi)}\right]$$

$$\cdot\, S\left(E - J^2/2mR^2 - mV_R\right)[1 - S(E)\,S(-v_r)] \qquad (6)$$

in which the unit step function

$$S(\delta) = \begin{cases} 1 & \delta > 0 \\ \\ 0 & \delta < 0 \end{cases},$$

V_R is the potential at r = R and the radial, latitudinal, and azimuthal components of the velocity $\vec{V}$ are given by

$$\left[\frac{2}{m}\left(E - J^2/2mR^2 - mV_R\right)\right]^{1/2},$$

$$\pm \frac{1}{mR}\left[J^2 - J_z^2/\sin^2\Theta\right]^{1/2},$$

$$J_z/mR\sin\Theta,$$

respectively, and where the ± sign corresponds to sgn v_θ at the exobase. For simplicity, the subscripts (i, j, k) on $(\Theta_{ij}, \Phi_{ijk})$ have been suppressed. The step function terms are analogous to those used by Aamodt and Case[4] and in I, in which case the step function multiplying the square bracket term admits only those trajectories having contact with the exobase while the term in square brackets removes all those particles exceeding the escape speed with negative radial velocities. Altogether then, the distribution function of Eq. (6) admits only those trajectories allowed on the model and satisfies the boundary dondition of Eq. (1). In addition, it is clear that the kinetic equation (2) is satisfied since the distribution is a function of the constants of the motion except for the term involving $S(v_r)$. It can be shown, by direct substitution into Eq. (2), that this term is an admissible solution (as shown similarly by Aamodt and Case).

The velocity moments of the distribution are formed by multiplying f of Eq. (6) by the appropriate velocities and integrating over all velocity space. We simplify the analysis by normalizing the exobase density and temperature distributions through

$$N(\Theta, \Phi) \equiv n_0 \nu(\Theta, \Phi), \quad T(\Theta, \Phi) = T_0 \tau(\Theta, \Phi),$$

where n_0 and T_0 are values of density and temperature at selected points on the exobase. As mentioned above, we consider a corotating exobase of angular velocity $\vec{\omega}$ directed along the polar axis and ignore the effects of other possible bulk flows just below the exobase by setting

$$(U_r,\ U_\theta,\ U_\phi) \ = \ (0,\ 0,\ \omega R \sin\Theta) .$$

It is worth mentioning at this point that differential rotation could be included here by letting $\omega = \omega(\Theta, \Phi)$. In addition, we make the spatial coordinate transformation

$$r \ = \ R\xi$$

and the velocity coordinate transformation

$$v_r \ = \ \gamma^{-1/2} x,\ v_\theta \ = \ \gamma^{-1/2} y,\ v_\phi \ = \ \gamma^{-1/2} z ,$$

in terms of the constant

$$\gamma \ = \ m / 2k T_0 .$$

Then, the general velocity moment of order (p, q, s), normalized to the base density n_0, is given by

$$\frac{n}{n_0} < v_r^p v_\theta^q v_\phi^s > \ = \ \mathcal{B}_{pqs}(\xi, \theta, \phi) + \mathcal{E}_{pqs}(\xi, \theta, \phi) , \qquad (7)$$

where the terms

$$\mathcal{B}_{pqs} \ = \ \frac{1}{\gamma^{\frac{p+q+s}{2}}} \sum_{i,\,j,\,k\,=\,1}^{2} \left(\int_0^{P_3} dx \int_0^{P_2} dz \int_0^{P_1} dy + \int_{P_3}^{P_6} dx \int_0^{P_5} dz \int_0^{P_4} dy \right)$$

$$\cdot \ \epsilon_i^p \, \epsilon_j^q \, \epsilon_k^s \, F_{ijk}(x, y, z, \xi, \theta, \phi,)$$

$$\mathcal{S}_{pqs} = \frac{1}{\gamma^{\frac{p+q+s}{2}}} \sum_{j,k=1}^{2} \left(\int_{P_3}^{P_6} dx \int_{0}^{P_5} dz \int_{P_4}^{P_1} dy + \int_{P_3}^{P_6} dx \int_{P_5}^{P_2} dz \int_{0}^{P_1} dy \right.$$

$$\left. + \int_{P_6}^{\infty} dx \int_{0}^{P_2} dz \int_{0}^{P_1} dy \right) \epsilon_j^q \epsilon_k^s F_{1jk}(x, y, z, \xi, \theta, \phi)$$

correspond to contributions from the bound and escaping trajectories, respectively. The limits of integration are given in terms of

$$\alpha = mMG/kT_0R = -2\gamma V_R ,$$

a measure of the gravitational energy relative to the thermal energy at the base, and

$$a = \alpha/\xi, \quad b = 1/(\xi^2 - 1), \quad d = a/(\xi + 1),$$

by

$$P_1 = (P_2^2 - z^2)^{1/2}, \quad P_2 = (bx^2 + d)^{1/2},$$

$$P_3 = \left[a(1 - 1/\xi)\right]^{1/2}, \quad P_4 = (P_5^2 - z^2)^{1/2},$$

$$P_5 = (a - x^2)^{1/2}, \quad P_6 = a^{1/2}.$$

The integrand function

$$F_{ijk} = \frac{\nu_{ijk}}{(\pi \tau_{ijk})^{3/2}} \exp\left\{ -\frac{1}{\tau_{ijk}} \left[x^2 + y^2 + z^2 + \alpha(1 - 1/\xi) \right.\right.$$

$$\left.\left. - 2\beta\xi \sin\theta \epsilon_k z + \beta^2 \sin^2\Theta_{ij} \right] \right\},$$

where

$$\beta = (m\omega^2 R^2 / 2kT_0)^{1/2} = \gamma^{1/2}\omega R$$

is a measure of the rotational kinetic energy relative to the thermal energy at the base, and $\nu_{ijk} \equiv \nu(\Theta_{ij}, \Phi_{ijk})$, and $\tau_{ijk} \equiv \tau(\Theta_{ij}, \Phi_{ijk})$.

For completeness, it is worth mentioning at this point that the moments of Eqs. (7) reduce to those obtained in I when the base temperature is taken to be uniform and the base density is taken to correspond to a rotating isothermal thermosphere (see Eq. (8) below). In addition, for the case of a nonrotating exosphere, $\beta = 0$, it can be shown through application of Liouville's theorem and appropriate coordinate transformations that Eqs. (7) reduce to the density[8] and radial flux[9] at the base, r = R, as derived by McAffee. And finally, taking $\beta = 0$ and $\tau_{ijk} = \nu_{ijk} = 1$, we obtain the density distribution of Öpik and Singer.[1-4]

The model considered here and in I is the usual minimum density model[1-5] in the sense that we ignore the possibility of bound orbiting particles (satellite particles) which do not intersect the base (see refs. 2, 11-13 for discussion of possible importance). The problem of determining the distribution of such particles is beyond the scope of this work (solution of kinetic equation which properly accounts for the production and loss of satellite particles through rare collision events and photoionization in the exosphere). One may include the contribution of satellite particles in an approximate way by simply adding a Maxwellian distribution f_M, truncated by $[1 - S(E - J^2/2mR^2 - mV_R)]\, S(-E)$, to Eq. (6). The temperature and density characterizing f_M could be taken as, say, those corresponding to the average values at the exobase.

III. NUMERICAL EXAMPLES

A. Model I

For purposes of brief review and comparison below, consider the model of I corresponding to a corotating, isothermal thermosphere where the exobase density distribution was given by

$$N = n_0 \exp (m\omega^2 R^2 \sin^2 \Theta_{ij} / 2kT_0), \tag{8}$$

exhibiting a density bulge at the equator. We note that this density, given in terms of the present model, leads to an exospheric distribution function f which is independent of (Θ_{ij}, Φ_{ik}). Consequently, the analysis in I was greatly simplified since detailed accounting of trajectories through such equations as (4) and (5) was unnecessary. In this case, the resulting profiles for density n and radial flux $n < v_r >$ simplify to a single quadrature over v_θ while $n < v_\theta >$ and $n < v_\phi >$ vanish (i.e., no lateral flow in exosphere).

To illustrate some of the main features of the model in I, consider the dashed lines of Fig. 1 where the normalized density n/n_0, at given colatitudes θ, is plotted versus ξ for the case $\alpha = 10$ and $\beta = 1$ (these values have been selected primarily for clarity of illustration and are used throughout this section). As shown in I, the density distribution along the polar axis ($\theta = 0$) is identical to the corresponding distribution of a nonrotating exosphere. We note, for a fixed radius, that the density increases from pole to equator. In other words, there is a density enhancement at all points in the exosphere for colatitudes $0 < \theta < \pi$. As noted in I, this variation results since particles are ejected with increasing azimuthal velocities for increasing colatitude so that the average altitude a particle attains in the equatorial region is greater than in the polar region,

leading to a higher density at the equator than the pole. In what follows, we designate this phenomena as the "centrifugal effect."

B. Uniform Density and Temperature

The conceptually simpler case of a corotating exobase with uniform density and temperature ($\nu_{ijk} = \tau_{ijk} = 1$) is computationally more difficult since f is a function of Θ_{ij} and Eq. (7) is required for the moments. Such an example of the density profile for $\alpha = 10$ and $\beta = 1$ is shown by the solid lines in Fig. 1. The dashed line, designated by $\theta = 0°$ (the same as model I), is the corresponding density profile for the nonrotating case, valid for all latitudes. As in the model of I with rotation, the density increases from pole to equator for a given radius. Again, we note a density enhancement in the equatorial region which is primarily due to the centrifugal effect. On the other hand, the values of density along the polar axis are lower than corresponding values of the nonrotating case. In fact the density is lower for a range of colatitudes about the poles.

This density reduction is consistent with the fact that there are now lateral winds in the exosphere flowing from the polar regions to the equatorial regions. Such lateral flow is expected in this case when a comparison is made with the isothermal model of I where no lateral flow occurs. In the latter model, the exobase density, given by Eq. (8), increases from pole to equator in a manner which is consistent with no lateral flow. Then, in the former case, there exists an "effective" density depletion in the equatorial region of the base, relative to the isothermal case of I, leading to flow from the polar region of effectively higher base density to the equatorial region of effectively lower base density.

C. Nonuniform Density

Taking the simple uniform model of subsection B as a point of departure, consider a rotating exosphere characterized by an exobase with uniform temperature ($\tau_{ijk} = 1$) and variable density. For simplicity, we choose an exobase density distribution which is rotationally symmetric about the x-axis ($\phi = 0$, $\theta = \pi/2$) with a sinusoidal density variation given by $\nu_{ijk} = N/n_0 = \left[1 - (1 - \epsilon_N) \cdot (1 + \epsilon_N)^{-1} \sin \Theta_{ij} \cos \Phi_{ijk}\right]$, which results in a density minimum on the equator at $\phi = 0$ and a density maximum at $\phi = \pi$. The ratio $\epsilon_N = N_{max}/N_{min}$, in terms of the maximum and minimum exobase densities.

Density profiles for a model exosphere of this kind, with $\epsilon_N = 1/3$ (chosen for clarity), are shown in Figs. 2 and 3 for $\phi = \pi$ and $\phi = 0$, respectively. In these figures $\alpha = 10$ and the solid lines are for a rotating planet with $\beta = 1$ while, for comparison, the dashed lines are for the corresponding nonrotating planet. In Fig. 2, note that the equatorial density is greater than the corresponding polar density at all altitudes above the exobase for both rotating and nonrotating models. This equatorial enhancement is in part a reflection of the exobase density maximum lying on the equator at this longitude. The ratio of equatorial to polar density is more pronounced in the rotating exosphere due to a combination of the centrifugal effect and lateral flow from regions of high to low exobase densities (actual and effective).

For the nonrotating case of Fig. 3, we note that the polar density is greater than the corresponding equatorial density at all altitudes, reflecting the base density minimum on the equator at this longitude. In contrast, the opposite relationship obtains for the rotating exosphere. That is, the equatorial density is

greater than the polar density at all altitudes above a crossover point $\xi_x \simeq 1.1$. In addition to the centrifugal effect, this density increase on the equator is due to the "rotationally enhanced" lateral transport of particles from exobase regions of higher densities. In fact, such a "mixing" of particles tends to equalize the density profiles around the planet on a given latitude as one can note in comparing the equatorial distributions of Figs. 2 and 3.

To further elucidate this rotationally enhanced mixing, consider Fig. 4, where a sketch of flux field lines $n < \vec{v} >$ are shown in the equatorial plane. For clarity, the relative number of field lines is not to scale since the flux decreases very rapidly with increasing ξ. We note the strong connection of field lines from one hemisphere to the other where a portion of the field lines from the high density base region feed back into regions of lower density while the remaining portion, corresponding to the escaping flux, form spirals which become radial as $\xi \to \infty$. The dashed lines shown indicate the approximate locus of points of maximum and minimum values of both flux and density for a given radial position. In this connection, we note that at about $\xi = 3$, the density (and flux) maximum is closer to the exobase density minimum than the maximum. This implies that the density at $\xi = 3$ should be greater above the base density minimum than the maximum; this is borne out by comparison of Figs. 2 and 3.

D. Nonuniform Temperature

We consider here the contrasting case of uniform base density ($\nu_{ijk} = \epsilon_N = 1$) and a rotationally symmetric base temperature distribution $\tau_{ijk} = T/T_0 = \left[1 + (1 - \epsilon_T)\,(1 + \epsilon_T)^{-1} \cdot \sin \Theta_{ij} \cos \Phi_{ijk}\right]$, in terms of $\epsilon_T = T_{min}/T_{max}$, the ratio of the minimum to maximum base temperatures. Then, for the nonrotating model shown in Fig. 5 (6), with $\epsilon_T = 1/2$, the equatorial density is

greater (less) than the corresponding polar density at all points above the base, this time reflecting the base temperature maximum (minimum) on the equator at this longitude. The same (opposite) relationship obtains in the rotating exosphere of Fig. 5 (6). In these cases, the temperature maximum and minimum play similar roles to the density maximum and minimum of the previous examples and the basic reasons for the differences between the rotating and nonrotating models are analogous.

IV. DISCUSSION AND CONCLUSIONS

The exobase distributions in density and temperature chosen for the numerical examples of section III correspond to the common idealization in which a density minimum and temperature maximum occur on the equator $\theta = \pi/2$ at the subsolar point $\phi = 0$ (approximate region of maximum solar extreme ultraviolet photoionization and heating) while a density maximum and temperature minimum occur at the anti-solar point (approximate region of maximum recombination and cooling). Then, to maximize the effects of rotation, the angular velocity $\vec{\omega}$ was directed along the polar axis. For purposes of illustration, the effects of variations in exobase density and temperature were considered separately but, of course, occur together in nature.

In the preceding examples we only considered the values $\alpha = 10$ and $\beta = 1$, since the general effects of variation of these parameters, as examined in I, still hold for the present nonuniform models. For example, a primary result noted in I is that the ratio of the equatorial density to the polar density, at a given altitude and longitude, increases when α, β, and ξ are increased separately or together. In addition, this ratio is greater than one for ξ greater than the crossover point ξ_x. In this connection, we point out that it can be shown that $\xi_x \to 1$ as β and/or α become large.

On comparing Figs. 2, 3, 5, and 6, one can note that the region of greatest exospheric density increase from the nonrotating to the rotating model occurs above points of base density or temperature minima. Further comparison with the uniform model of Fig. 1 shows that the corresponding rotational density enhancement is less than that of the nonuniform models (above base density and

temperature minima). Altogether then, the effects of rotation appear to be more important in nonuniform exospheres.

With the model developed here we can now estimate the equatorial density enhancement (region where most prominent) of terrestrial hydrogen and helium due to rotation. For this purpose we choose the distributions $\tau_{ij} = 1 + 0.28 \cdot \cos^{2.5}(Z_{ijk}/2)$ and $\nu_{ijk} = 1 - (1/3) \cos Z_{ijk}$ (here $\cos Z_{ijk} = \sin \Theta_{ij} \cos \Phi_{ijk}$) used by Wallace, et al.[14] to fit the observed hydrogen density from Lyman α data. In addition, we assume that the exobase is corotating with $\omega = 1.02 \times 10^{-4}$ sec^{-1}, the observed atmospheric (super) rotation rate[15] near the exobase for the range $30° \lesssim \theta \lesssim 150°$; i.e., 1.4 times the rotation rate of Earth. In this case, with R = 6880 km and $T_0 = 805°K$, we obtain a 15 to 17 percent increase in hydrogen density above that of the nonrotating model for the range of 10 to 20 earth radii.

The corresponding density enhancement in terrestrial helium is 40 to 80 percent over the range 1.7 to 2 planetocentric radii, the region where helium becomes a minor constituent. However, recent observations indicate that there is a helium density bulge over the winter pole.[16] In this case, distributions of the form $\nu_{ij} = 1 + .82 \cos \Theta_{ij}$ and $\tau_{ij} = 1$ may be more realistic. On this basis, taking $T_0 = 1000°K$, we still obtain a rather large density enhancement of 30 to 50 percent on the equator for ξ of 1.7 to 2.

The numerical examples considered in this paper assume that appropriate sources and sinks exist in the thermosphere to allow the resulting flow of particles across the exobase. The flow is limited by the maximum rate at which the species in question can diffuse in the thermosphere. No quantitative

limitations can be determined for the examples of Sec. III until a planet and species are specified. However, for the terrestrial hydrogen and helium examples of this section, the maximum allowable diffusive fluxes, as estimated by McAfee,[8] are about 8.9×10^7 $cm^{-2}sec^{-1}$ and 5.4×10^8 $cm^{-2}sec^{-1}$, respectively. In these cases, we obtain maximum allowable exobase densities of 5×10^4 cm^3 (somewhat lower than the expected value $\sim 10^5$ cm^3) and 5×10^6 cm^3 (expected value $\sim 10^6$ cm^3) for hydrogen and helium.

Exosphere models of the kind presented here assume a Maxwellian velocity distribution at the exobase. This assumption is self-consistent with respect to the distribution of bound particles, $E < 0$, when the exobase is uniform. On the other hand, as is well known, the distribution has a "hole" corresponding to the absence of those particles with $E > 0$ and $v_r < 0$, leading to a flux (and density) discontinuity across the exobase, the Jeans escape flux. With a nonuniform exobase, even the distribution of bound returning particles, $E < 0$ and $v_r < 0$, is not Maxwellian in form, leading to further discontinuity in density and flux across the exobase. But, when variations in density and temperature occur just below the exobase, flow is expected in the thermosphere and should be reflected in the exobase distribution. The possibility for such flow was included in the general distribution of Eq. (6).

In the context of this model, one cannot expect to remove the density and flux discontinuity corresponding to those particles in the range $E > 0$ due to the complete absence of such particles with $v_r < 0$. However, since bound returning particles ($E < 0$, $v_r < 0$) are present, it is logical to expect that it should be possible to remove or reduce the discontinuities in flux and density of the class

of particles with $E < 0$ by balancing the flux just below the base (bound particles only) with the flux $n_0 (\mathcal{B}_{100}\,\hat{r} + \mathcal{B}_{010}\,\hat{\theta} + \mathcal{B}_{001}\,\hat{\phi})$ just above (conservation of flux). For example, when the density and temperature are given at the base, the balancing can be accomplished through successive approximations to $\vec{U}(\Theta, \Phi)$. To test this procedure and get an indication of the effects of including bulk velocity $\vec{U}$, we performed approximate hand calculations to balance the flux across the base (10 percent accuracy) for the examples of Fig. 2. We found that the density discontinuity was reduced and the density profiles were essentially unchanged for $\gamma > 10^{-13}$ (over the range considered $1 \leq \xi \leq 10$). When γ was reduced to 10^{-14}, we found both increases and decreases in the density by about 10 percent at $\xi = 10$; such changes being smaller for $\xi < 10$ and vanish as $\xi \to 1$. In addition, the maximum outward radial bulk velocities U_r were 5×10^4 cm/sec and 1×10^5 cm/sec when γ was 10^{-13} and 10^{-14}, respectively. Also note that, when $U_r > 0$ on this model, the modified Jeans escape flux $n_0 \mathcal{E}_{100}$ is greater than the corresponding value when $U_r = 0$, which may result in important increases in estimates of planetary loss rates.

The degree to which the base can be nonuniform on this model and still lead to meaningful solutions is unknown. As done previously for the uniform model,[17-19] this problem can be resolved by a full kinetic treatment of the exobase region, taking proper account of the transition from the collision dominated thermosphere to the collisionless exosphere. It is clear, of course, that the accuracy of the model improves in the limit of a uniform exobase, in which case $\vec{U} \to 0$ (distribution of bound particles becomes Maxwellian at base).

ACKNOWLEDGMENTS

I wish to thank Dr. S. J. Bauer for useful discussions during the course of this investigation. I also thank Mr. P. Smidinger and Mr. E. Victor for performing the numerical integrations.

REFERENCES

1. E. J. Öpik and S. F. Singer, Phys. Fluids 2, 653 (1959).

2. E. J. Öpik and S. F. Singer, Phys. Fluids 4, 221 (1961).

3. J. Herring and J. Kyle, J. Geophys. Res. 66, 1980 (1961).

4. R. E. Aamodt and K. M. Case, Phys. Fluids 5, 1019 (1962).

5. K. M. Hagenbuch and R. E. Hartle, Phys. Fluids 12, 1551 (1969).

6. J. A. Burke, Mon. Not. R. Astr. Soc. 145, 487 (1969).

7. T. M. Donahue and G. E. Thomas, J. Geophys. Res. 68, 2661 (1963).

8. J. R. McAfee, Ph.D. thesis, University of Pittsburg (1965).

9. J. R. McAfee, Planet. Space Sci. 15, 599 (1966).

10. R. R. Hodges, Jr. and F. S. Johnson, J. Geophys. Res. 73, 7307 (1968).

11. J. C. Brandt and J. W. Chamberlain, Phys. Fluids 3, 485 (1960).

12. E. J. Öpik and S. F. Singer, Phys. Fluids 3, 486 (1960).

13. J. W. Chamberlain, Planet. Space Sci. 11, 901 (1963).

14. L. Wallace, C. A. Barth, J. B. Pearce, K. K. Kelly, D. E. Anderson, Jr., and W. G. Fastie, J. Geophys. Res. 75, 3769 (1970).

15. D. G. King-Hele, Nature 226, 439 (1970).

16. C. A. Reber, D. N. Harpold, R. Horowitz, A. E. Hedin, J. Geophys. Res. 76, 1845 (1971).

17. M. Liwshitz and S. F. Singer, Planet. Space Sci. 14, 541 (1966).

18. J. W. Chamberlain and F. J. Campbell, Astrophys. J. 149, 687 (1967).

19. R. T. Brinkmann, Planet. Space Sci. 18, 449 (1970).

FIGURE CAPTIONS

Fig. 1. The normalized density n/n_0 at colatitudes $\theta = 0°, 45°, 90°$ versus the normalized radius $\xi = r/R$ for values $\alpha = mMG/kT_0R = 10$ and $\beta = (m\omega^2R^2/2kT_0)^{1/2} = 1.0$. The dashed lines are the isothermal model of I and the solid lines are for the model with uniform base density and temperature.

Fig. 2. The normalized density n/n_0 at colatitudes $\theta = 0°, 90°$, longitude $\phi = 180°$ versus the normalized radius $\xi = r/R$ for values $\alpha = mMG/kT_0R = 10$, $\beta = (m\omega^2R^2/2kT_0)^{1/2} = 0$ (dashed lines), 1.0 (solid lines), and $\epsilon_N = N_{min}/N_{max} = 1/3$.

Fig. 3. The normalized density n/n_0 at colatitudes $\theta = 0°, 90°$, longitude $\phi = 0°$ versus the normalized radius $\xi = r/R$ for values $\alpha = mMG/kT_0R = 10$, $\beta = (m\omega^2R^2/2kT_0)^{1/2} = 0$ (dashed lines), 1.0 (solid lines), and $\epsilon_N = N_{min}/N_{max} = 1/3$.

Fig. 4. Sketch of field lines $n < \vec{v} >$ in the equatorial plane for counterclockwise rotation. The maximum exobase density is indicated by H and the minimum by L. The dashed lines to the right (left) are the approximate locus of both density and flux maxima (minima) for a given altitude.

Fig. 5. The normalized density n/n_0 at colatitudes $\theta = 0°, 90°$, longitude $\phi = 0°$ versus the normalized radius $\xi = r/R$ for values $\alpha = mMG/kT_0R = 10$, $\beta = (m\omega^2R^2/2kT_0)^{1/2} = 0$ (dashed lines), 1.0 (solid lines), and $\epsilon_T = T_{min}/T_{max} = 1/2$.

Fig. 6. The normalized density n/n_0 at colatitudes $\theta = 0°$, $90°$, longitude $\phi = 180°$ versus the normalized radius $\xi = r/R$ for values $\alpha = mMG/kT_0R = 10$, $\beta = (m\omega^2R^2/2kT_0)^{1/2} = 0$ (dashed lines), 1.0 (solid lines), and $\epsilon_T = T_{min}/T_{max} = 1/2$.

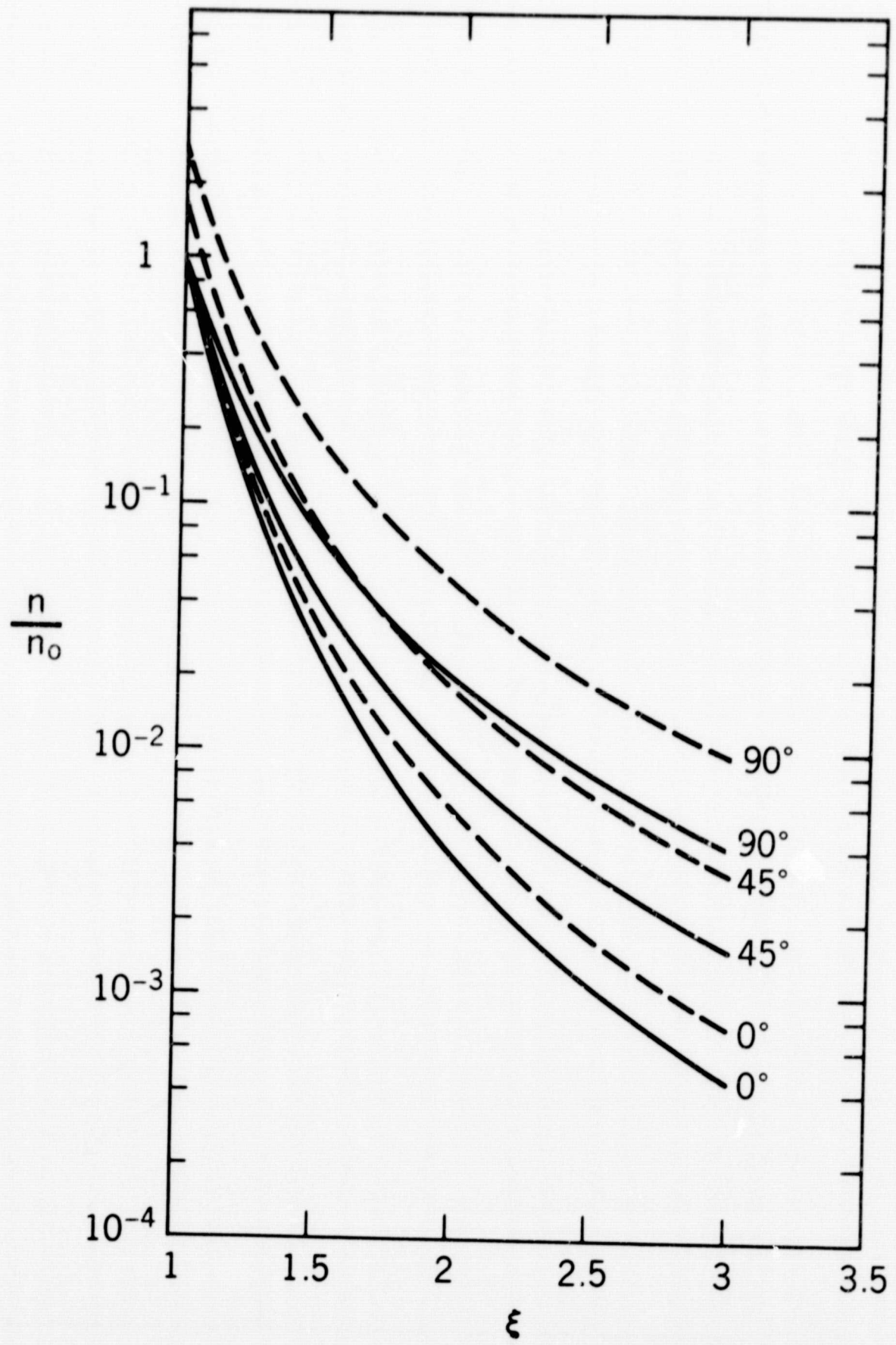

Figure 1

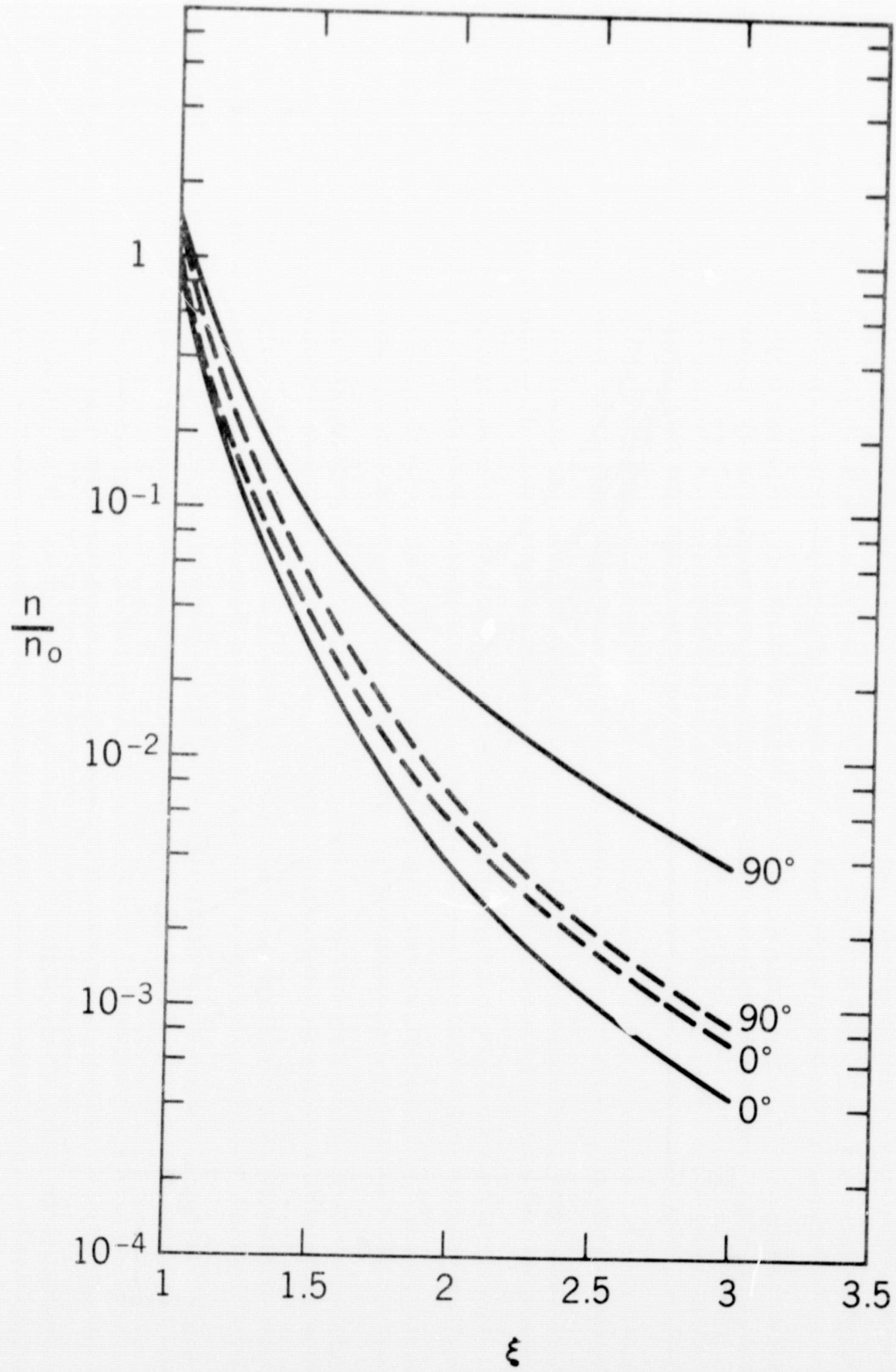

Figure 2

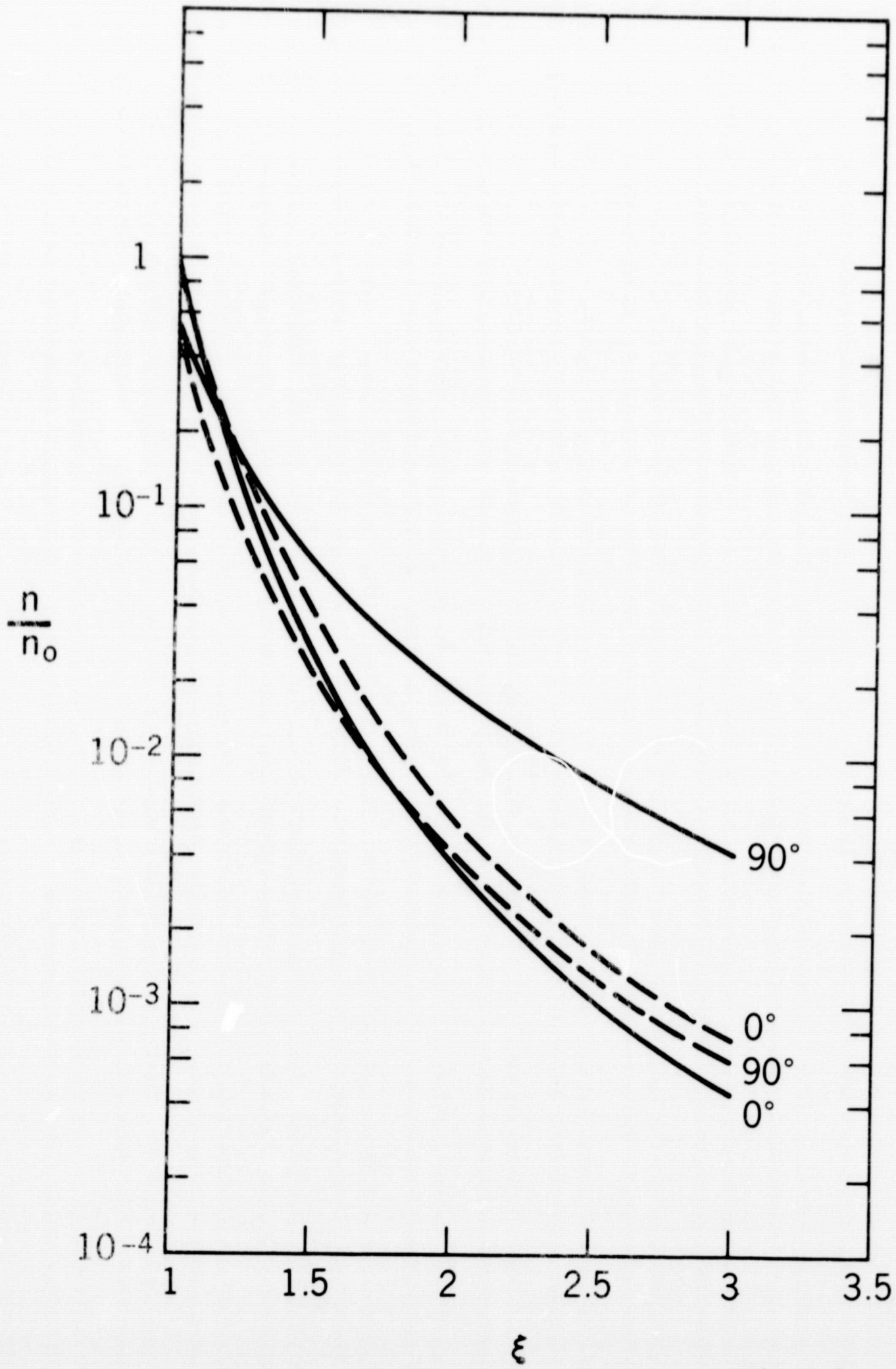

Figure 3

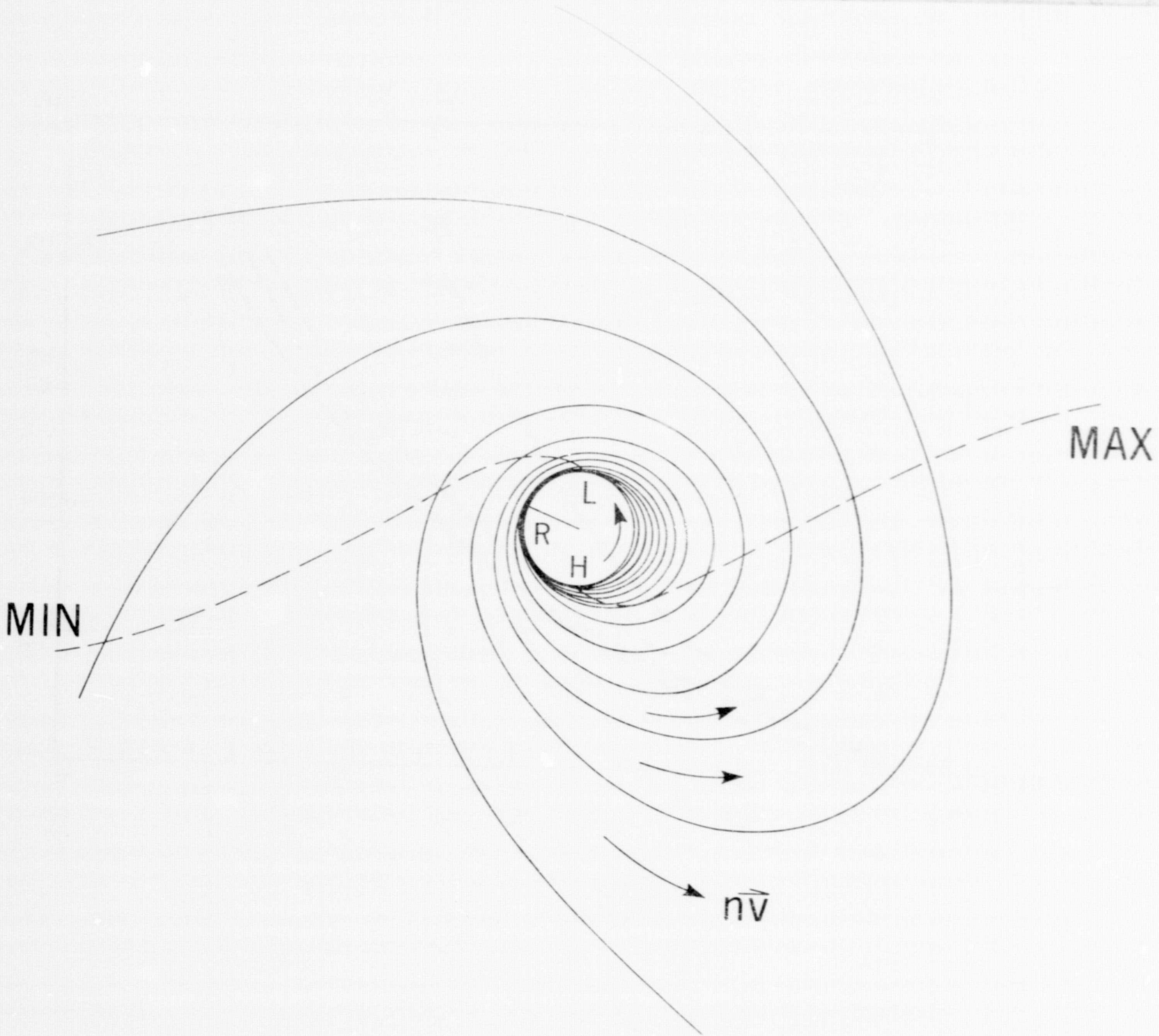

Figure 4

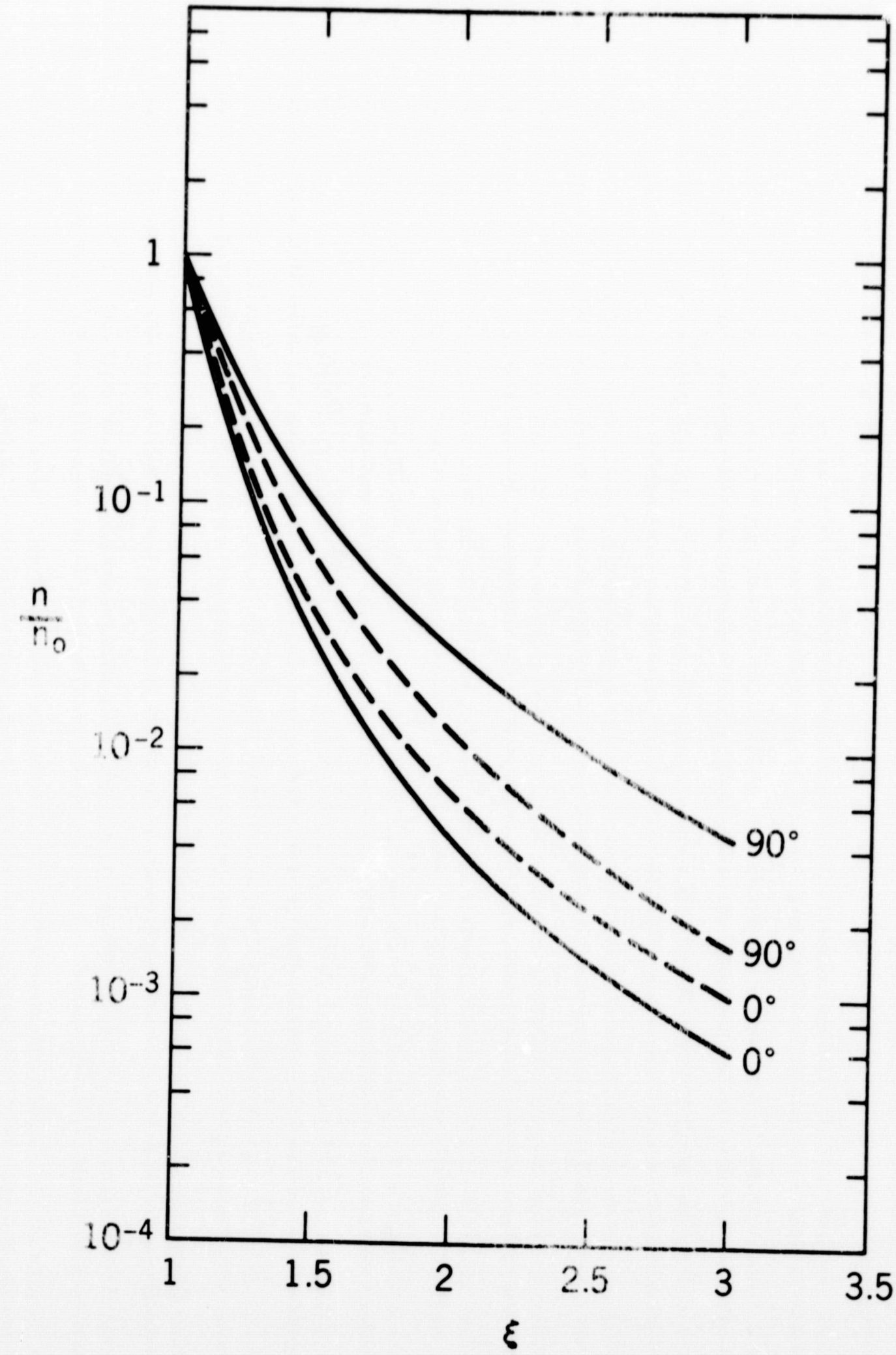

Figure 5

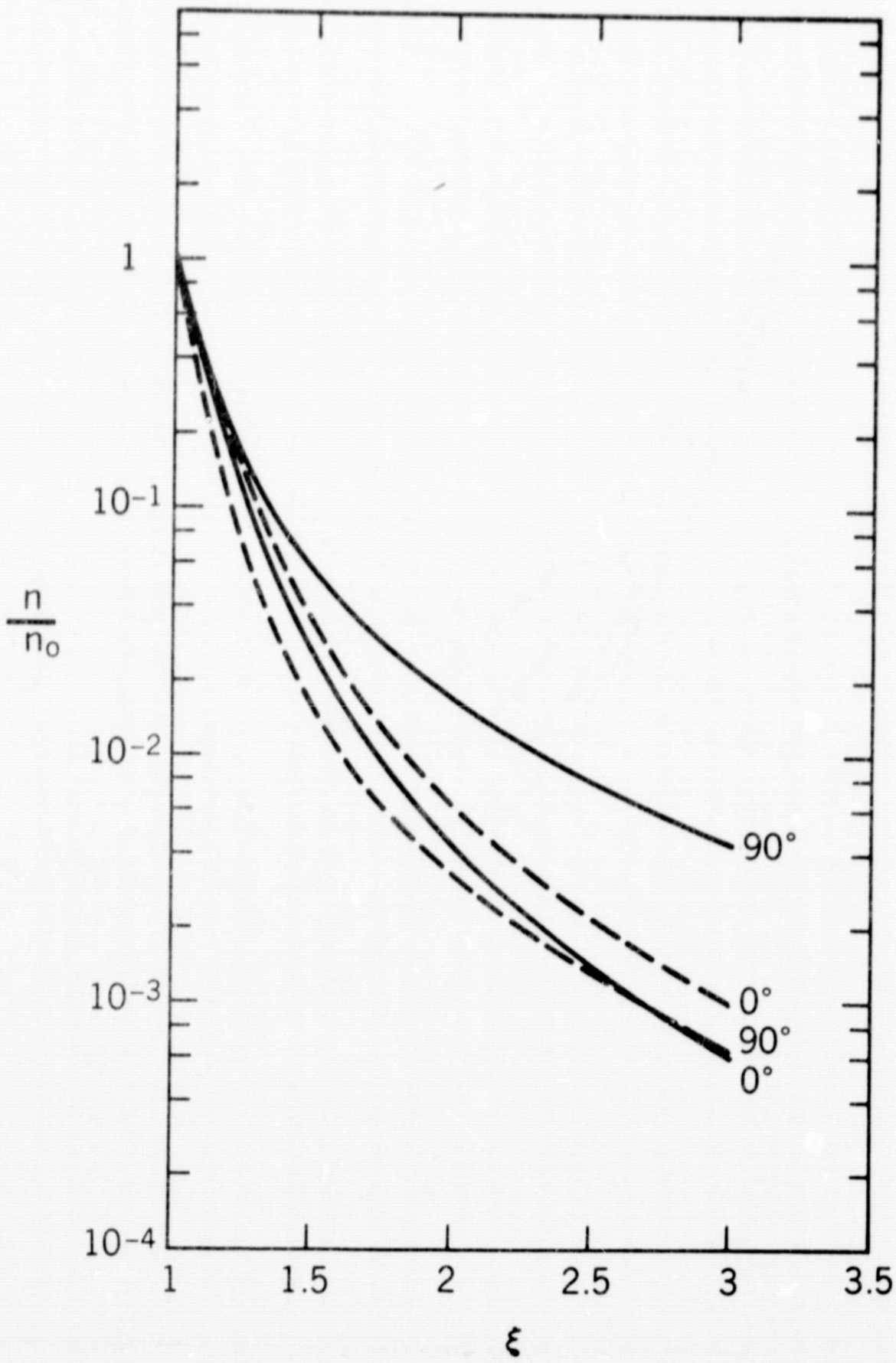

Figure 6